

Low power In Memory Computation with Reciprocal Ferromagnet/Topological Insulator Heterostructures

Hamed Vakili,^{1,*} Samiran Ganguly,² George J. de Coster,³ Mahesh R. Neupane,^{3,4} and Avik W. Ghosh^{1,2}

¹Department of Physics, University of Virginia, Charlottesville, VA 22904, USA

²Department of Electrical and Computer Engineering, University of Virginia, Charlottesville, VA 22904, USA

³DEVCOM Army Research Laboratory, 2800 Powder Mill Rd, Adelphi, MD, 20783, USA

⁴Materials Science and Engineering Program, University of California, Riverside, CA, 92521, USA

(Dated: March 30, 2022)

The surface state of a 3D topological insulator (3DTI) is a spin-momentum locked conductive state, whose large spin hall angle can be used for the energy-efficient spin orbit torque based switching of an overlying ferromagnet (FM). Conversely, the gated switching of the magnetization of a separate FM in or out of the TI surface plane, can turn on and off the TI surface current. The gate tunability of the TI Dirac cone gap helps reduce its sub-threshold swing. By exploiting this reciprocal behaviour, we can use two FM/3DTI heterostructures to design a 1-Transistor 1-magnetic tunnel junction random access memory unit (1T1MTJ RAM) for an ultra low power Processing-in-Memory (PiM) architecture. Our calculation involves combining the Fokker-Planck equation with the Non-equilibrium Green Function (NEGF) based flow of conduction electrons and Landau-Lifshitz-Gilbert (LLG) based dynamics of magnetization. Our combined approach allows us to connect device performance metrics with underlying material parameters, which can guide proposed experimental and fabrication efforts.

In-memory computing or Processing-in-Memory (PiM) [1, 2] is an important emerging architectural design that reduces data movement between the memory and the processor. PiM operates by performing simple intermediate steps along a long chain of compute processes within the memory array itself, as far as possible. The memory layout in a typical PiM architecture is in the form of a grid. Each row and column of the grid is driven by selectors, which enable the cells for a read or write operation. A sense amplifier reads an entire row of the memory cell by comparing its state against a known reference voltage, current, or charge [3]. While such a local computing paradigm leads to a significantly reduced footprint, this however, needs to be traded off against material integration complexity as well as overall switching costs.

Recent experiments on spin-orbit torque (SOT) based switching [4–7] in FM/3DTI heterostructures have shown TIs to be a promising alternative to heavy metal (HM) underlayers, because of their higher spin Hall angle. Conversely, the ability of a FM to turn current ON or OFF in a TI by breaking inversion symmetry through its orientation [8, 9] offers an option for a gate tunable selector, along with the intrinsic energy efficiency of a gate-tunable bandgap [10]. This brings up intriguing possibilities of using the reciprocal interactions between a FM and a TI to realize unique, energy-efficient device configurations.

In this paper we present a potentially energy efficient efficient 1-Transistor 1-magnetic tunnel junction random access memory unit (1T1MTJ-RAM), that can function as the building block of a PiM design (Fig. 1). In the device we are proposing, there are two FM/3DTI heterostructures, one functioning as a transistor switch/row-column selector, and the other as a nonvolatile memory

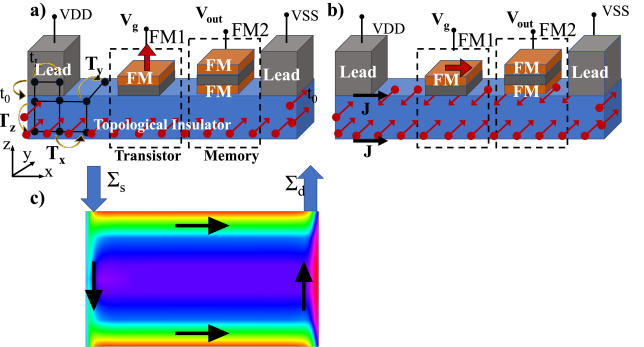


FIG. 1. a) Schematic 1T1MTJ cell using FM/3DTI heterostructure in the off state, where a ferromagnet FM1 oriented perpendicular to the TI plane opens a gap in its top surface states. The source and drain are placed on top of the channel region in contact with the top layer. b) In the ON state of the device, the current flow at the top surface is restored upon rotating the magnetization FM1 into the TI plane, whereupon the TI top surface bandstructure is no longer gapped. c) Simulated current flows on both top and bottom layers, connected by current flowing along the un-gapped side walls. The first ferromagnet (FM1) is the selector unit while the second (FM2) is the memory unit.

unit. The switching in the second, MTJ memory unit (FM2) is based on conventional spin orbit torque (SOT) [4–6], with the required spin current at the FM2-3DTI interface provided by the spin momentum locking at the 3DTI surface. The FM that acts as the transistor unit (FM1) is the trickier component, as it needs to be electrically switched from out of plane to in plane and back. There are a number of mechanisms to achieve this transistor like behaviour. One way is to use a gated piezoelectric clamped above a magnetostrictive material sit-

* hv8rf@virginia.edu

ting on the TI [11–16]. Another mechanism is interface induced anisotropy of a FM/3DTI and an applied electric field to control the polarization of the FM1 [17, 18]. The latter approach benefits from intrinsic properties of the FM/3DTI heterostructure and the effect of Voltage Controlled Magnetic Anisotropy (VCMA) [19].

One of the known challenges for the FM1-3DTI is an expected low On/Off ratio compared to competing technologies such as CMOS. In this paper we show that as a selector for low power PiM, the On/Off ratio does not need to be very high. In fact, our proposed device is naturally suited for compact PiM designs, since it directly incorporates a selection transistor in the first FM1-3DTI combination. Using an enhanced sense-amplifier for each column with programmable sensing thresholds, it is possible to implement basic Boolean operations (AND, OR, XOR, Majority, and their complements). We describe a possible scheme of building such a PiM towards the end.

Computational approach. We set up a tight binding Hamiltonian that describes the 3DTI, the Zeeman energy term H_Z originating from the FM/3DTI exchange and the on-site energy term H_V from the applied gate voltage at FM1, with parameters fitted to *ab-initio* calculations. In the 3D atomistic grid $\{i, j, k\}$, this looks like [20–23]

$$\begin{aligned} H &= H_{3DTI} + H_Z + H_V & (1) \\ H_{3DTI} &= \sum_{ijk} c_{i,j,k}^\dagger \varepsilon_{3DTI} c_{i,j,k} + \left(c_{i,j,k}^\dagger T_x c_{i+1,j,k} + \right. \\ &\quad \left. c_{i,j,k}^\dagger T_y c_{i,j+1,k} + c_{i,j,k}^\dagger T_z c_{i,j,k+1} + h.c. \right) \\ H_Z &= \sum_{ijk} c_{i,j,k}^\dagger M_0 \mathbf{S} \cdot \boldsymbol{\sigma} c_{i,j,k} \\ H_V &= \sum_{ijk} c_{i,j,k}^\dagger V_g(x_i, z_k) c_{i,j,k} \end{aligned}$$

where the onsite energies $\varepsilon_{3DTI} = (C_0 + 2C_1 + 4C_2)I_{4 \times 4} + (M + 2M_1 + 4M_2)I_{2 \times 2} \otimes \tau_z$, while the various hopping terms $T_{x,y} = -M_2 I_{2 \times 2} \otimes \tau_z - C_2 I_{4 \times 4} + (iA_0/2)\sigma_{x,y} \otimes \tau_x$, $T_z = -M_1 I_{2 \times 2} \otimes \tau_z + C_1 I_{4 \times 4} + (iB_0/2)\sigma_z \otimes \tau_x$. For Bi₂Se₃, the parameters used are $M = 0.28$ eV, $A_0 = 0.8$ eV, $B_0 = 0.32$ eV, $C_1 = 0.024$ eV, $C_2 = 1.77$ eV, $M_1 = 0.216$ eV, $M_2 = 2.6$ eV, $C_0 = -0.0083$ eV. τ and σ are the Pauli matrices in orbital and spin subspaces respectively while I is the identity matrix. One layer each of the source and drain is included in the Hamiltonian. The fixed FM in the MTJ is not included in the simulation.

The employment of a 3D model allows us to separate the bulk and interfacial components of the charge and current distribution. The placements of magnets and the source and drain contacts are shown in Fig. 1. The current source, drain, the FM1 and FM2 are all connected to the top surface.

We employ the Non-Equilibrium Green's Function (NEGF) formalism to analyse the transport signatures and the overall performance of the device. The retarded Green's function G^r and correlation (i.e., non-equilibrium) Green's function G^n of the electron can be

written as [24, 25]

$$\begin{aligned} G^r(E, \mathbf{k}_\perp) &= [EI - H(\mathbf{k}_\perp) - \Sigma_S(E, \mathbf{k}_\perp) - \Sigma_D(E, \mathbf{k}_\perp)]^{-1} \\ G^n(E, \mathbf{k}_\perp) &= G^r(f_S \Gamma_S + f_D \Gamma_D) G^{r\dagger} \\ \Gamma_{S,D} &= i \left(\Sigma_{S,D} - \Sigma_{S,D}^\dagger \right) \end{aligned} \quad (2)$$

with $f_{S,D}$ the bias separated Fermi-Dirac distribution functions on the source/drain sides. We assumed an infinite cross-section that allowed us to Fourier transform the transverse y-z hopping terms into \vec{k}_\perp . The self-energies $\Sigma_{S,D}$ describe the projection of the contact states onto the channel, and are calculated recursively at each energy and transverse momentum value. $\Gamma_{S,D}$ are the corresponding energy broadening matrices denoting escape rates into the contacts. The charge and spin currents from site i to j are then calculated as

$$J_s^{i \rightarrow j} = \frac{q}{ih} \sum_{\mathbf{k}_\perp, E} \text{Tr} [\boldsymbol{\sigma} (H_{ij} G_{ji}^n - G_{ji}^n H_{ij})] \quad (3a)$$

$$J_q^{i \rightarrow j} = \frac{q}{ih} \sum_{\mathbf{k}_\perp, E} \text{Tr} [(H_{ij} G_{ji}^m - G_{ji}^m H_{ij})] \quad (3b)$$

The SOT torque is given by $\tau_{SOT} = \mathbf{m} \times (\mathbf{J}_p \times \mathbf{m}) - \alpha \mathbf{m} \times \mathbf{J}_p$, where α is the Gilbert damping and \mathbf{m} is the magnetization vector of the ferromagnet. The polarization current \mathbf{J}_p comes from the NEGF calculated spin current \mathbf{J}_s in the TI, as well as phenomenological scattering terms in the magnet. We can keep track of the separate in and out of plane vector components of the polarization current as a complex vector, $\mathbf{J}_p = \mathbf{J}_{in} + i\mathbf{J}_{out}$, where [26–29]:

$$\mathbf{J}_p = \frac{p \mathbf{J}_s \lambda^2}{t} \left(\frac{1}{\lambda_\phi^2} - \frac{i}{\lambda_j^2} \right) \frac{\cosh t/L - 1}{\sinh t/L} \quad (4)$$

where the net scattering length $\lambda = (1/\lambda_{sr}^2 + 1/\lambda_\phi^2 - i/\lambda_j^2)^{-1/2}$. $\lambda_{sr}, \lambda_\phi, \lambda_j$ are spin relaxation, precessional and decoherence length of the ferromagnet of thickness t . J_s is the spin current density at the interface of FM2 and TI calculated from Eq. 3b, and p is the efficiency of spin current transfer from TI to FM2 (taken to be 0.1 here), which depends on the interfacial exchange. Note that due to the spin current precessing in the ferromagnet, an out of plane component arises in the torque, denoted by the imaginary part of τ_{SOT} .

The dynamics of the two magnets are simulated using the Landau-Lifshitz-Gilbert (LLG) equation[30]. By changing the anisotropy we can switch FM1 from out of plane to in plane (using VCMA or strain), which changes the Zeeman Hamiltonian H_Z . The corresponding NEGF calculated torque τ_{SOT} with phenomenological corrections (Eqs. 3b,4) is then fed into the LLG equation self-consistently. Assuming the electron transit speed is orders of magnitude faster than the magnet's characteristic FMR frequency, we can stick to steady state NEGF, and adjust the torque quasi-statically as the magnetization \mathbf{m} evolves. The quasi-static approximation reduces computational complexity significantly without compromising on accuracy. The bandstructure of the 3DTI at

the location of the FM1 is modified due to the interfacial effects and the applied voltage, which shift its location with respect to the Fermi energy (Fig. 2). The shift of bandstructure is not uniform throughout the thickness; we shift the bottom surface 0.5 times the top surface under the applied gate voltage V_g , and assume the magnet covers the full TI width laterally.

To solve the LLG equation we have taken a macro spin model with effective anisotropy field $\mathbf{H}_K = (2\Delta k_B T/M_s V)(\mathbf{u}_0 \cdot \mathbf{m})\mathbf{u}_0$, where Δ is the ferromagnet's thermal stability, related to anisotropy K as $\Delta = KV/k_B T$. \mathbf{u}_0 is the effective field, pointing along \hat{z} and \hat{y} directions for FM1 and FM2 respectively at the start of the simulation. For room temperature simulations we have added a stochastic effective field described as $\mathbf{H}_{Th} = (\eta/\mu_0)\sqrt{2\alpha k_B T/M_s \gamma V \Delta t}$ [31], where η is a random vector following a normal distribution with zero average. μ_0 is vacuum permeability, α is damping, k_B is Boltzmann constant, T is temperature, M_s is saturation magnetization, γ is the electron gyromagnetic ratio. V and Δt are volume of FM2 and simulation time step. Finally, the solved LLG equation can be written as: $(1 + \alpha^2)\partial_t \mathbf{m} = \gamma(\mathbf{m} \times \mathbf{H} + \alpha \mathbf{m} \times (\mathbf{m} \times \mathbf{H}) + \tau_{SOT})$, with $\mathbf{H} = \mathbf{H}_K + \mathbf{H}_{Th}$.

The voltage control of the FM1 anisotropy can come from a VCMA effect across an oxide-FM stack, with coefficient ξ and oxide thickness t_{ox} . Here $\Delta K_u = \xi V/t_{ox} t_{FM}$ due to the electric field from the vertical voltage difference across the stack and the interfacially induced anisotropy. Alternatively, if we use strain as a switching mechanism for FM1, the applied effective field can be added to \mathbf{H} as $\zeta(\mathbf{u} \cdot \mathbf{m})\mathbf{u}$ [16] where ζ is the strain coefficient that needs to cancel out the effective anisotropy field \mathbf{H}_K . \mathbf{u} is the strain direction which needs to be along \mathbf{z} (perpendicular to the TI) in this case. A third mechanism for controlling the anisotropy is by varying the free energy [17] through an applied gate voltage. This method works by making the perpendicular FM1 with gapped 3DTI the favorable state compared to in-plane FM1 and gapless 3DTI. For the VCMA mechanism, assuming a thickness of 1 nm for the capped oxide and FM1 layers, a $\Delta K_u/V = 100 KJ/m^3$ for CoFeB of 1 nm thickness has been reported [32, 33], whereas by doping FM/oxide interface larger $\Delta K_u/V$ has been achieved as well [34, 35]. For the straining mechanism, $\Delta K_u/V$ of 200-300 KJ/m^3 have been reported [16]. For both the VCMA and strain mechanism, the free energy change from the applied gate V_g can potentially lower the voltage requirements. The required voltage to change the anisotropy of a reliable FM1 with $\Delta = 40$ of size $40 \times 40 \times 1 \text{ nm}^3$ would be 0.3-1 V. Although this would be relatively large compared to the applied bias because there would be negligible current flowing in the FM1 heterostructure, the energy consumption would still be small (in the range of 100 aJ [16]).

Results: In Fig. 2 we look at the bandstructure of the 3DTI channel under four circumstances. Fig 2a and b show the bandstructure of the channel at the location of

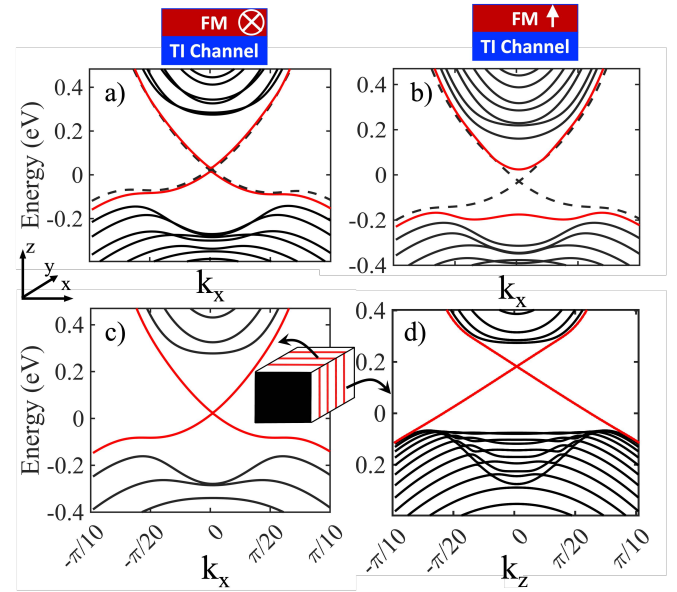


FIG. 2. The band structure of the device channel at various points. Red lines in (a-c) emphasize the top surface states and in d, the side surfaces. Dashed lines show the bottom surface states a) FM/3DTI bandstructure with in plane magnet (in y direction) b) Magnet in z direction with on site voltage energy at the top at -0.1 and bottom at -0.05 V. c) Bandstructure of the pristine (magnet free) 3DTI channel discretized in the z direction (top to bottom) d) Bandstructure of the 3DTI channel discretized in the transport direction (side to side).

the FM1, for the On (magnet in plane of TI) and Off (magnet out of plane) states respectively, while Fig. 2c shows the pristine (magnet-free) TI states for comparison. For the On state, we see a small modification of band-structure in (a). Specifically, the Dirac point is shifted away from the Γ point. For the Off state (b) however, the degeneracy is lifted and a corresponding energy gap is created for the states arising from the top surface (solid lines), while at the same time keeping the bottom surface states (dashed lines) intact. We also present the side surface states (Fig. 2. d) and as expected (Fig. 1.b) the sides of the 3DTI stay gapless for both On and Off states, as the FM only affects part of the top surface. This would mean that for an electrical transistor based on FM/3DTI [17], the current along the 3DTI sides would play a crucial role. However in the device geometry we propose here, we avoid the problem of dealing with the side current as only the top surface states can apply any appreciable spin orbit torque to FM2.

For a competitive transistor-memory device based on the FM/3DTI stack, we outline requirements in this paper. The first is the On/Off ratio β . For deterministic switching of an in-plane ferromagnet with a given thermal barrier Δ , the critical spin current is estimated as $I_s = (4q\alpha k_B T \Delta / \hbar)$ [36]. We also need to make sure that when FM1 is out-of-plane in the Off state, the surface leakage current would be small enough to not acciden-

tally switch FM2. The probability of switching P can be approximated from a Fokker-Planck analysis with a perpendicular magnet [37, 38]

$$P = \exp(-\pi^2/4W),$$

$$W = \frac{1}{\Delta} \left[e^{2\tau\iota} \left(1 + \frac{1}{\iota} \right) - \frac{1}{\iota} \right]$$

$$\tau \equiv \frac{\alpha\gamma\mu_0 H_K}{1 + \alpha^2} t \quad (5)$$

When the TI is not gapped (FM1 in plane, $P \approx 1$), the write error is $WER \approx 1 - P$, while when the TI is locally gapped (FM1 out of plane, $P \approx 0$), the error is $WER \approx P$. For simplicity we take the WER in both cases to be equal to each other. In the case of thermally assisted switching (Off) we would need to either solve the Fokker Planck equation or use the empirical equation $P = \exp(-tf_0 \exp(-\Delta(-t)^c))$, where t is the switching time, and $\iota = I/I_s - 1$ is the fractional current overdrive. c is an empirical constant between 1 and 2, where 1 is for in-plane and 2 is for out-of-plane FM2, and in between for imperfect materials.

The ability to open a gap is determined by the Zeeman term $H_z = M_0 \mathbf{S} \cdot \boldsymbol{\sigma}$ which breaks the time reversal symmetry. This term needs to be large enough to have a small error rate for accidental switching. Equation 5 allows the material parameters to be directly connected to the device performance metrics. For long term storage, we assume $\Delta = 40$, write error rate $WER = 10^{-7}$, $c = 1.2$ [39, 40] and attempt frequency $f_0 = 1 \text{ GHz}$ [41]. For the Off state, depending on the required memory application (e.g. cache memory or long term memory) t would be different, ranging from $\sim \mu\text{s}$ to years. We can see from Fig. 3.a that depending on the values of V_g and M_0 , the device can be used in different regimes. When the FM1 is in plane, the required I/I_s is 1.7. When FM1 is out plane, the flowing current needs to be small enough to not accidentally switch FM2. For short term memory, this requires I/I_s to be < 0.2 . This means that a modest On/Off ratio of 10 would make the device work. For longer memory applications (hours to days), a larger On/Off ratio (Fig. 3a), $\log_{10} \beta > 3$ is needed.

From Figs. 2c and d we can see there is a band offset between the side and top surface TI bandstructures. This would mean that the conductivity of side and top surfaces differ at any given energy. To achieve minimum required magnetic exchange M_0 , the applied gate voltage should be approximately at the midpoint of this band offset, $V_g \approx (E_D^{Top} - E_D^{Side})/2$, where $E_D^{Top} = 0 \text{ eV}$ and $E_D^{Side} = 0.17 \text{ eV}$ are the Dirac points of the top and side bands respectively. This matches the observation from Fig. 3a, where the minimum M_0 required for short term ($\sim \mu\text{s}$) memory happens when the V_g is near the midpoint (red dashed line). This implies that without a magnetization, when the chemical potential is tuned to the top or side Dirac point to reduce its conductivity, the other surface will retain a large density of states (DOS), providing a shunting conduction channel. For long term

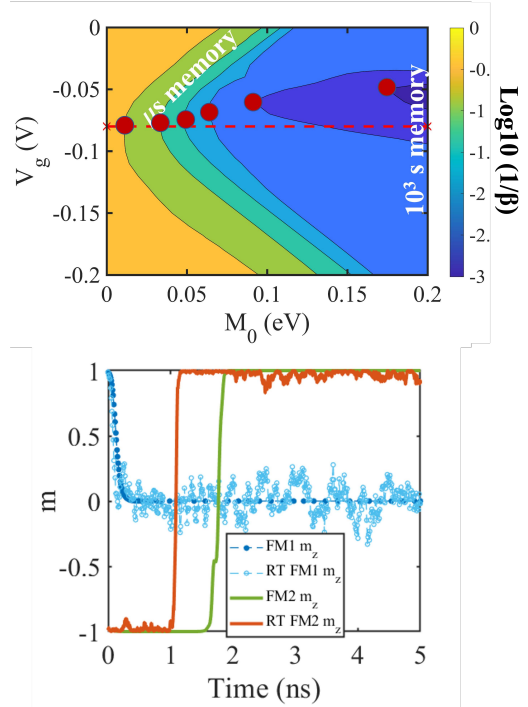


FIG. 3. The colorplot shows the logarithm of the On/Off ratio β of non-equilibrium spin current J_s at the FM2/3DTI interface with respect to the Zeeman energy coefficient M_0 and applied gate bias V_g . The contours show different memory regimes in which the device can operate, ranging from cache memory (operating in μs up to longer term memory, like a computer RAM 10^3 s). The dashed red line is the V_g midway between the top and side band offsets. As explained in the text, the red circles show the minimum required M_0 for each contour. Bottom figure shows the 0 K and 300 K simulation of the FM2 magnetization dynamics. Applied voltage bias and V_g are 100 mV. The Zeeman exchange energy for FM2 is taken to be 10 meV. λ_{sr} , λ_ϕ , λ_j are taken to be 1, 10, 1 nm respectively. Source, drain, FM1 and FM2 lengths are 20 nm each. 3DTI thickness is 5 nm (6 layers) and magnet thickness t is 2 nm. The total length of the channel is 140 nm. Gilbert damping α is 0.1.

(10^3 s) memory, a higher On/Off ratio is needed which requires a bigger bandgap, hence a larger M_0 value. Due to the sizable gap opening for long term memory, the critical V_g for the minimum required M_0 deviates from the midpoint.

Note that the required On/Off ratio would be larger if we used a simplified 2D Hamiltonian that only considers the surface states. This is because in a realistic TI structure, a significant amount of the current shunts into the bulk of the TI stack [31], which our 3D geometry naturally takes into account (current shunting seen in Fig. 1c - we simulate a depth of 6 layers here). To have a faster working memory, using a perpendicular ferromagnet as FM2 is preferred, as the switching mechanism would be determined by a field like torque which is faster than an anti-damping torque. However, for a perpendicular

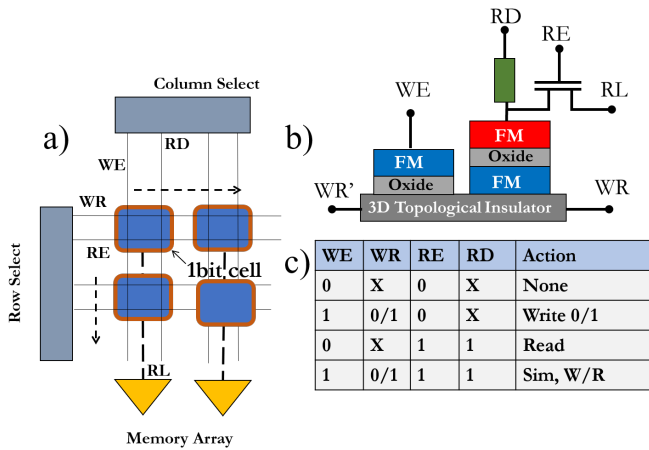


FIG. 4. a. Memory array for the presented cell b. The cell and its position in the array indicated. c. The truth table for the array operations.

ferromagnet an assisting external field is required. This assisting field can originate from the stray field of a capping magnetic layer or the exchange bias of a coupled antiferromagnet-ferromagnet stack [42–44].

Proposal for a Processor-in-Memory (PiM) design. In Fig. 4a. we show a possible approach for performing in-memory compute functions using an array built out of the presented memory cell. The relation between the voltage lines in Fig. 4 and 1 are as follows: $WR : VDD$, $WR' : VSS$, $WE : Vg$, $RL : V_{out}$. The cell (Fig. 4b) contains a selection transistor, which acts as a write enable, i.e. WE signal. The current flowing in the TI acts as the write signal, with the two ends being designated as WR and WR' . Since a spintronic memory cell requires bipolar currents for programming, we can either use a bipolar current generating selector to drive the WR signal with WR' grounded, or else reverse the polarities of WR, WR' pairs between 0/1 and 1/0 respectively.

The read is performed through a voltage divider arrangement at the reader MTJ, which changes the output voltage at the read line (RL) that is shared over the cells in the array column-wise. This reader is charged through the RD line, and we include one transistor in the cell for a read enable functionality (RE) that also provides the load resistance which attaches a meaningful current quantity to the read line per cell depending on the voltage at the divider; critical for the read and PiM functionalities as we describe next. We choose to arrange the read to be done row-wise, whereas the write is done column-wise. This is by no means a necessary condition for designing this architecture, but simply one of the choices we make that allows us the option of simultaneous read and write options, if it is ever necessary. The read process is performed by sensing the current in the

read line and compared with a reference current in the sense amplifier (SA), which then reports the value stored at a specific cell addressed via RD and RE signals. The truth table of these operations is shown in Fig. 4c.

The processing-in-memory functions are also arranged within the SA over each column. We can build in reference currents that enable Boolean operations over the whole array by enabling multiple rows at the same time. Consider a two-bit AND operation over any two rows. In this case, the two specific rows are enabled using RE and all the RD over the rows are enabled as well. Each of the SA reference currents for the AND operation is set to $1.8I_R$ where I_R is the read current of a cell when it is storing ‘1’. In this case both of the cells being read simultaneously by a single SA will have to be ‘1’ to trigger the SA to report ‘1’, in all other combinations it will report ‘0’. Similarly for the OR case, the reference current can be set as $0.8I_R$ to trigger ‘1’ from SA for even one of the cells being ‘1’. An XOR gate can be implemented by a two threshold SA where the thresholds are $0.8I_R$ and $1.8I_R$ and it is configured to report ‘1’ when reading values in between these two references. The complement functions are easily implemented by using an additional inverter. All these functionalities are built within a single SA and as per the requirements of the computation the SA can be configured to perform a given operation.

Conclusion. In this letter we have proposed an in-memory processing device based on FM and 3DTI. The main advantage these two components provide is in their potential ultra low power operation. We have used Fokker-Planck with NEGF-LLG simulations to directly connect the device performance to material parameters. Furthermore, we have shown that even though the On/Off ratio of FM/3DTI is lower than conventional CMOS devices, a modest On/Off ratio is sufficient for certain types of applications. Overall, there are a few fundamental obstacles for such a device which need to overcome to be realized. One which is the low On/Off ratio of the FM/3DTI which we have addressed in this letter. Second is for the case where a PMA magnet is used for FM2 which can be faster than the in-plane switching. For PMA switching with inplane polarization, an assisting in-plane field perpendicular to spin current polarization is needed. A magnetic field as an assisting field is not practical in a real device. Alternate methods need to be explored such as using AFM exchange biasing or perhaps another FM layer to rotate the spin current polarization from its original direction.

Acknowledgments. We acknowledge useful discussions with Patrick Taylor (ARL), Joe Poon (UVA) and Supriyo Bandyopadhyay (VCU). This work is supported by the Army Research Lab (ARL) and in part by the NSF I/UCRC on Multi-functional Integrated System Technology (MIST) Center; IIP-1439644, IIP-1439680, IIP-1738752, IIP-1939009, IIP-1939050, and IIP-1939012.

[1] P. Chi, S. Li, C. Xu, T. Zhang, J. Zhao, Y. Liu, Y. Wang, and Y. Xie, in [2016 ACM/IEEE \(ISCA\)](#) (2016) pp. 27–39.

[2] S. Ghose, A. Boroumand, J. S. Kim, J. Gómez-Luna, and O. Mutlu, [IBM Journal of Research and Development](#) **63**, 3:1 (2019).

[3] X. Fong, Y. Kim, K. Yogendra, D. Fan, A. Sengupta, A. Raghunathan, and K. Roy, [IEEE Transactions on Computer-Aided Design of Integrated Circuits and Systems](#) **35**, 1 (2016).

[4] A. R. Mellnik, J. S. Lee, A. Richardella, J. L. Grab, P. J. Mintun, M. H. Fischer, A. Vaezi, A. Manchon, E.-A. Kim, N. Samarth, and D. C. Ralph, [Nature](#) **511**, 449.

[5] Y. Wang, D. Zhu, Y. Wu, Y. Yang, J. Yu, R. RamaSwamy, R. Mishra, S. Shi, M. Elyasi, K.-L. Teo, Y. Wu, and H. Yang, [Nat Commun](#) **8**, 1364.

[6] J. Han, A. Richardella, S. A. Siddiqui, J. Finley, N. Samarth, and L. Liu, [Phys. Rev. Lett.](#) **119**, 077702.

[7] J. Han and L. Liu, [APL Materials](#) **9**, 060901.

[8] Y. G. Semenov, X. Duan, and K. W. Kim, [Phys. Rev. B](#) **86**, 161406.

[9] T. Taniyama, [J. Phys.: Condens. Matter](#) **27**, 504001.

[10] K. Wang, M. M. Elahi, L. Wang, K. M. M. Habib, T. Taniguchi, K. Watanabe, J. Hone, A. W. Ghosh, G.-H. Lee, and P. Kim, [Proceedings of the National Academy of Sciences](#) **116**, 6575 (2019), <https://www.pnas.org/doi/pdf/10.1073/pnas.1816119116>.

[11] C. A. F. Vaz, F. J. Walker, C. H. Ahn, and S. Ismail-Beigi, [J. Phys.: Condens. Matter](#) **27**, 123001.

[12] M. Trassin, [J. Phys.: Condens. Matter](#) **28**, 033001.

[13] P. Manchanda, U. Singh, S. Adenwalla, A. Kashyap, and R. Skomski, [IEEE Transactions on Magnetics](#) **50**, 1 (2014).

[14] E. De Ranieri, P. E. Roy, D. Fang, E. K. Vehstedt, A. C. Irvine, D. Heiss, A. Casiraghi, R. P. Campion, B. L. Gallagher, T. Jungwirth, and J. Wunderlich, [Nature Mater](#) **12**, 808.

[15] R. Verba, I. Lisenkov, I. Krivorotov, V. Tiberkevich, and A. Slavin, [Phys. Rev. Applied](#) **9**, 064014 (2018).

[16] S. Bandyopadhyay, J. Atulasimha, and A. Barman, [Applied Physics Reviews](#) **8**, 041323 (2021).

[17] Y. G. Semenov, X. Duan, and K. W. Kim, [Phys. Rev. B](#) **86**, 161406 (2012).

[18] X. Duan, X.-L. Li, X. Li, Y. G. Semenov, and K. W. Kim, [Journal of Applied Physics](#) **118**, 224502 (2015).

[19] S. Manipatruni, D. E. Nikonorov, C.-C. Lin, B. Prasad, Y.-L. Huang, A. R. Damodaran, Z. Chen, R. Ramesh, and I. A. Young, [Science Advances](#) **4**, eaat4229 (2018).

[20] C.-X. Liu, X.-L. Qi, H. Zhang, X. Dai, Z. Fang, and S.-C. Zhang, [Phys. Rev. B](#) **82**, 045122 (2010).

[21] M. Götte, T. Paananen, G. Reiss, and T. Dahm, [Phys. Rev. Applied](#) **2**, 054010 (2014).

[22] P. Sengupta, T. Kubis, Y. Tan, and G. Klimeck, [Journal of Applied Physics](#) **117**, 044304 (2015).

[23] J. Liu and T. Hesjedal, [Advanced Materials](#) , 2102427.

[24] S. Datta, [Lessons from Nanoelectronics](#) (WORLD SCIENTIFIC, 2012).

[25] A. Ghosh, [Nanoelectronics - a Molecular View](#) (WORLD SCIENTIFIC, 2016).

[26] A. Manchon, R. Matsumoto, H. Jaffres, and J. Grollier, [Phys. Rev. B](#) **86**, 060404 (2012).

[27] P. B. Ndiaye, C. A. Akosa, M. H. Fischer, A. Vaezi, E.-A. Kim, and A. Manchon, [Phys. Rev. B](#) **96**, 014408 (2017).

[28] M. H. Fischer, A. Vaezi, A. Manchon, and E.-A. Kim, [Phys. Rev. B](#) **93**, 125303 (2016).

[29] A. K. Reza, X. Fong, Z. A. Azim, and K. Roy, [IEEE Transactions on Electron Devices](#) **63**, 1359 (2016).

[30] J. Slonczewski, [Journal of Magnetism and Magnetic Materials](#) **159**, L1 (1996).

[31] H. Vakili, Y. Xie, S. Ganguly, and A. W. Ghosh, [arXiv:2110.02641 \[cond-mat\]](#) (2021), arXiv: 2110.02641.

[32] S. Kanai, M. Yamanouchi, S. Ikeda, Y. Nakatani, F. Matsukura, and H. Ohno, [Applied Physics Letters](#) , 122403 (2012).

[33] F. Xue, N. Sato, C. Bi, J. Hu, J. He, and S. X. Wang, [APL Materials](#) **7**, 101112 (2019).

[34] B. Rana and Y. Otani, [Communications Physics](#) **2**, 90 (2019).

[35] T. Nozaki, T. Yamamoto, S. Miwa, M. Tsujikawa, M. Shirai, S. Yuasa, and Y. Suzuki, [Micromachines](#) **10**, 327 (2019).

[36] J. Z. Sun, [Phys. Rev. B](#) **62**, 570 (2000).

[37] W. H. Butler, T. Mewes, C. K. A. Mewes, P. B. Visscher, W. H. Rippard, S. E. Russek, and R. Heindl, [IEEE Transactions on Magnetics](#) **48**, 4684 (2012).

[38] Z. Li and S. Zhang, [Phys. Rev. B](#) **69**, 134416 (2004).

[39] D. Bedau, H. Liu, J.-J. Bouzaglou, A. D. Kent, J. Z. Sun, J. A. Katine, E. E. Fullerton, and S. Mangin, [Applied Physics Letters](#) **96**, 022514 (2010).

[40] H. Liu, D. Bedau, J. Sun, S. Mangin, E. Fullerton, J. Katine, and A. Kent, [Journal of Magnetism and Magnetic Materials](#) **358-359**, 233 (2014).

[41] L. Breth, D. Suess, C. Vogler, B. Bergmair, M. Fuger, R. Heer, and H. Brueckl, [Journal of Applied Physics](#) **112**, 023903 (2012).

[42] V. Krizakova, K. Garello, E. Grimaldi, G. S. Kar, and P. Gambardella, [Applied Physics Letters](#) **116**, 232406 (2020).

[43] W. J. Kong, C. H. Wan, X. Wang, B. S. Tao, L. Huang, C. Fang, C. Y. Guo, Y. Guang, M. Irfan, and X. F. Han, [Nat Commun](#) **10**, 233.

[44] Z. Zheng, Y. Zhang, V. Lopez-Dominguez, L. Sánchez-Tejerina, J. Shi, X. Feng, L. Chen, Z. Wang, Z. Zhang, K. Zhang, B. Hong, Y. Xu, Y. Zhang, M. Carpentieri, A. Fert, G. Finocchio, W. Zhao, and P. Khalili Amiri, [Nat Commun](#) **12**, 4555.